

Seasonal and interannual variability of the North Equatorial Current, the Mindanao Current, and the Kuroshio along the Pacific western boundary

Bo Qiu and Roger Lukas

Department of Oceanography, University of Hawaii at Manoa, Honolulu

Abstract. Along the Philippine coast in the western Pacific, the North Equatorial Current (NEC) bifurcates into the northward flowing Kuroshio and the southward flowing Mindanao Current. Using both the linear, time-dependent Sverdrup theory and a high-resolution, nonlinear reduced-gravity model, this study investigated the changes in the NEC-Mindanao Current-Kuroshio (NMK) system induced by large-scale surface wind forcings. Using the Florida State University monthly wind stress data from 1961 through 1992, we show that the seasonal bifurcation of the NEC occurs at the northernmost position in October and the southernmost position in February. While the meridional migration of the basin-wide trade wind has a relatively small effect in shifting the bifurcation latitude (by about 100 km), the monsoonal wind along the low-latitude western Pacific is effective in inducing a large northward excursion of the NEC's bifurcation in the fall season. On the interannual timescale, the positive wind stress curl of the trade wind tends to intensify and shifts the zero wind stress curl line northward prior to El Niño-Southern Oscillation (ENSO) events. With a lag of about 1 year this shift induces the bifurcation of the NEC to occur at a higher latitude. During the La Niña years the NEC generally bifurcates at a lower latitude. No significant seasonal fluctuations are found in the transport of the NEC near the Philippine coast. Seasonal changes in the Mindanao Current and the Kuroshio are, however, significant, and their transports tend to fluctuate 180° out of phase, due to the different speeds of the baroclinic Rossby waves at their respective latitudes. The Kuroshio (the Mindanao Current) has a seasonal minimum (maximum) transport in fall when the NEC bifurcates at the seasonally northernmost latitude. The interannual changes in the inflow NEC are largely controlled by the basin-wide, wind stress curl anomalies. While the quasi-biennial changes are confined only to the southern limb of the NMK system, signals with ENSO timescales are found to influence the midlatitude, subtropical circulation via the Kuroshio.

Introduction

After encountering the western boundary along the Philippine coast, the North Equatorial Current (NEC) in the Pacific Ocean bifurcates into the northward flowing Kuroshio and the southward flowing Mindanao Current (Figure 1) [Nitani, 1972]. If the surface wind forcing is steady, it is easy to show from the Sverdrup dynamics that the NEC's bifurcation should occur where the zonally averaged transport stream function is zero. In reality, the surface wind field changes both in time and in space and these changes can exert a particularly large impact upon the NEC-Mindanao Current-

Kuroshio (NMK) system near the Pacific's western boundary. This is because locally wind-forced Sverdrup disturbances in the tropical and subtropical interior oceans move preferentially westward and their influence eventually accumulates at areas near the western boundary [e.g., Lighthill, 1969]. In addition to these remote wind forcings, the east Asian monsoon, extending along the low-latitude western boundary of the Pacific, is also likely to directly impact the NMK system.

General descriptions of the NMK current system have been provided by several previous studies. Using hydrographic data from various cruises between 1934 and 1968, Nitani [1972] showed the bifurcation of the NEC at the sea surface occurs at 11°N to 14.5°N and that it tends to shift to the north with increasing depth. On the basis of water mass distributions along the western boundary and in the NEC, Toole *et al.* [1988] estimated the NEC's bifurcation at a latitude around

Copyright 1996 by the American Geophysical Union.

Paper number 95JC03204.
0148-0227/96/95JC-03204\$09.00

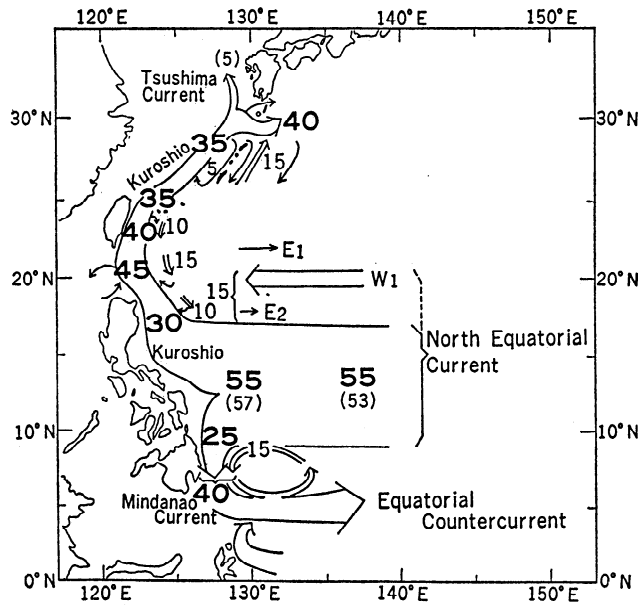


Figure 1. Schematic chart of geostrophic volume transport relative to 1200 dbar-depth in the North Equatorial Current-Mindanao Current-Kuroshio (NMK) system [from Nitani, 1972]. Values are in Sverdrup ($10^6 \text{ m}^3 \text{ s}^{-1}$).

12°N . Wyrski [1961] derived the seasonal pictures of the surface NMK system using data from the *Snellius* and *Dana* expeditions and from other Indonesian and Japanese observations. He found that while there was no clear seasonal signal in the inflow NEC near the western boundary, the baroclinic transport of the Kuroshio (the Mindanao Current) was larger (smaller) in spring months than in fall months.

Using the daily sea level data from tide gauges at Davao and Malakal, Lukas [1988] inferred that the transport of the Mindanao Current is dominated by interannual fluctuations and that an intermittent quasi-biennial variation is more prominent than variations associated with the El Niño-Southern Oscillation (ENSO) events. On the basis of high-resolution conductivity-temperature-depth (CTD) data and an inverse method, Toole *et al.* [1990] found a twofold increase in the NMK's transport in spring 1988 as compared with fall 1987; the inflow NEC in the upper thermocline increased from 32 to 61 Sv, the Mindanao Current from 14 to 30 Sv, and the Kuroshio from 12 to 31 Sv. Similar large-amplitude transport fluctuations in the NMK system were also noted by Cannon [1970], Hu and Cui [1991], and Wijffels *et al.* [1995] in their respective analyses of multiyear, in-situ observations (see Lukas *et al.* [1991, Table 1] for a summary of the Mindanao Current's transport estimated by various previous investigators). In particular, Wijffels *et al.* showed that large transport changes of the Mindanao Current were associated with the presence of warm-core features east of the Mindanao Current.

Understanding the NMK current system is important for an accurate estimation of the heat and freshwater transport away from the tropical Pacific. It is

also important because it directly connects the tropical and subtropical ocean circulations. Regarding the tropical/subtropical gyre interactions, McCreary and Lu [1994] recently presented an interesting study in which they emphasized the role played by the "subtropical cell" that advects the warm and relatively fresh, tropical surface water to midlatitudes, subsurfaces there due to the Ekman pumping, and returns colder and saltier subtropical water back to the subsurface tropics. Mass and heat exchange between the tropical and subtropical gyres in the North Pacific can also occur, due to the fluctuations in the NMK current system. Evidence for this has recently been given by Bingham and Lukas [1994] and Fine *et al.* [1994], who showed that part of the North Pacific Intermediate Water is able to penetrate into the tropical circulation through the Mindanao Current. The interannual variability in the NEC may also influence the subtropical circulation in the midlatitude. By comparing the time series of subsurface temperature across the Kuroshio Extension with that of the sea level difference across the NEC, Yamagata *et al.* [1985] showed that a significant correlation exists between the interannual changes of the two currents; the changes of the Kuroshio Extension are found to lag behind those of the NEC by about 1.5 years.

Because of its importance for regional and possibly basin-scale circulations, a thorough study with a focus upon the NMK system is clearly warranted. It is worth mentioning that such current bifurcations near western boundaries exist in other oceans. The South Pacific South Equatorial Current (SEC) bifurcates at the Great Barrier Reef into the East Australian Current and the New Guinea Coastal Undercurrent [Church, 1987]. The SEC in the South Atlantic bifurcates at the coast of Brazil into the northward North Brazil Coastal Current and the southward Brazil Current [Metcalf, 1968]. The SEC in the Indian Ocean bifurcates into the northward Somali Current and southward Agulhas Current. Because the bifurcation process is so general, a solid understanding of it in the North Pacific will help to understand how it works in the other oceans as well.

Although the existing studies based on hydrographic, sea level, and surface drifter data in the North Pacific have provided a general description of the circulation pattern, our understanding of the variability of the NMK system remains still limited. This is largely due to the lack of measurements with temporally continuous and spatially extensive coverage in the NMK region. In the past decade many studies using numerical models have advanced our understanding of the seasonal and interannual variations in the low-latitude Pacific Ocean [Busalacchi and O'Brien, 1980, 1981; Philander *et al.*, 1987; Kubota and O'Brien, 1988; McPhaden *et al.*, 1988; Kindle *et al.*, 1989; Inoue and Welsh, 1993; among others]. While many of these studies have investigated the basin-scale changes in the low-latitude Pacific Ocean, few works have focused on the NMK system. In this study, using both a simple analytical model

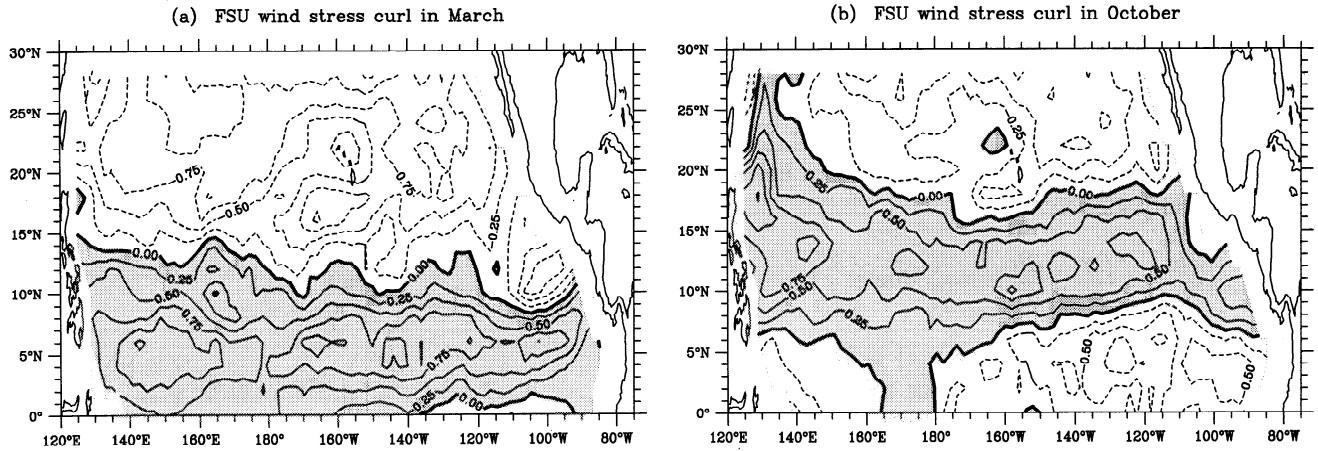


Figure 2. Surface wind stress curl values calculated from the Florida State University (FSU) wind climatology (1961–1992) for (a) March and (b) October. Shaded areas denote positive values of $\nabla \times \vec{\tau}$, and contour intervals are $0.25 \times 10^{-7} \text{ Nm}^{-3}$.

driven by an idealized surface wind pattern and a non-linear, high-resolution, reduced-gravity model forced by the Florida State University (FSU) wind data from 1961 through 1992, we will address the following questions: (1) What are the changes in the bifurcation latitude of the NEC and what are the important physical processes controlling these changes? (2) How do NEC fluctuations partition transport between the Kuroshio and the Mindanao Current? (3) How is the variability in the NMK current system related to the basin-scale variability of the low-latitude Pacific Ocean?

Theoretical Background

Before going into the details of the numerical model, it is beneficial to investigate the bifurcation of the NEC near the western boundary using linear dynamics. Such

an investigation can serve as a guideline for our more complicated modeling efforts because it helps establish the relationship between the fluctuations of the surface wind field, its frequencies and latitudinal migration, and the NEC’s bifurcation latitude. Although the focus of this section will be on the seasonal wind, the argument can be easily extended to include interannual wind changes. Figure 2 shows the surface wind stress curl field in March and October from the FSU wind climatology. Since the curl field is mostly zonal, a more convenient way of looking at the basin-scale, seasonal wind fluctuations is to plot the zonally averaged wind stress curl values as a function of time (Figure 3a). As signified by the zero contour centered around 15°N, the observed boundary between the tropical and subtropical wind belts migrates seasonally with an amplitude of 4° latitude. Given the large-scale wind fluctuations

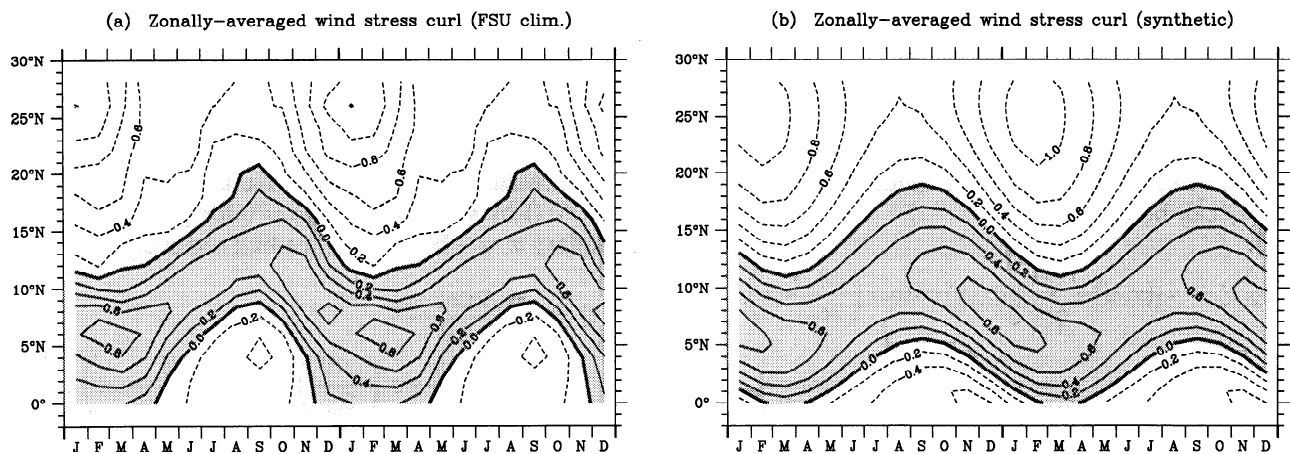


Figure 3. (a) Zonally averaged wind stress curl values as a function of month. The values are computed from the monthly FSU wind climatology from 1961 to 1992. For clarity, the monthly values are plotted for a 2-year time period. (b) Wind stress curl values computed using the analytical form of (2). The parameters are chosen such that the resultant wind stress curl approximates the observed field shown in Figure 3a. Here $A = 0.2 [1 + 0.025(y + 8^\circ)] \times 10^{-7} \text{ Nm}^{-3}$, $B = 3.5A$, $\phi = 60 \text{ days}$, $L(y) = 40^\circ / (1 - 0.05y)$, and $\alpha = 4^\circ$.

shown in Figure 3a, what is the response at the ocean's western boundary? Would the oceanic gyre boundary migrate with the same amplitude and phase as the wind stress curl field?

To answer these questions, we consider below the time-dependent, β -plane ocean response in a linearized reduced gravity model:

$$\frac{\partial h}{\partial t} - \left(\frac{\beta c^2}{f^2} \right) \frac{\partial h}{\partial x} = -\frac{1}{\rho_0} \nabla \times \left(\frac{\vec{\tau}}{f} \right). \quad (1)$$

[cf. Meyers, 1979], where $h(x, y, t)$ is the height deviation from the mean upper layer thickness H_0 , $\vec{\tau}$ is the vector of the surface wind stress, f is the Coriolis parameter, and β is the y derivative of f . In (1), $c = (g'H_0)^{1/2}$ is the speed of internal gravity waves, where g' is the reduced gravity. The right hand side of (1) consists of the following two terms: $-(\nabla \times \vec{\tau})/f\rho_0$ and $\beta\tau^x/f^2\rho_0$. Amplitudes in the seasonal changes of $\nabla \times \vec{\tau}$ and τ^x are typically $0.8 \times 10^{-7} \text{ N m}^{-3}$ and 0.03 N m^{-2} in the region under consideration (see Figure 3a for the $\nabla \times \vec{\tau}$ values). Near the NEC's bifurcation latitude ($\sim 15^\circ\text{N}$) the ratio of these two terms, $|\beta\tau^x/f(\nabla \times \vec{\tau})|$, is about 0.2, suggesting the wind stress curl change will dominate the time evolution of the h field. For simplicity of the following argument, only the $-(\nabla \times \vec{\tau})/f\rho_0$ term is retained in this section.

As depicted in Figure 3b, the observed seasonally fluctuating wind stress curl field (Figure 3a) can be very well represented by the following function:

$$\nabla \times \vec{\tau} = -\{A \cos[\omega(t - \phi)] + B\} \sin \left[\frac{2\pi}{L}(y + \alpha \cos \omega t) \right] \quad (2)$$

where y is relative to the latitude of the mean $\nabla \times \vec{\tau} = 0$ (15°N for the tropical/subtropical North Pacific) and $t = 0$ corresponds to January 1. In (2), ϕ denotes the time when the wind stress curl reaches its maximum after January 1, L is the meridional wavelength of the tropical/subtropical wind belts, $\omega = 2\pi/1 \text{ year}$, and α is the amplitude of the zero wind stress curl line's north-south migration.

Given the synthetic wind stress curl field of (2), the forced ocean response from the potential vorticity equation (1) can be expressed by

$$h(x, y, t) = a_0(x, y) + \sum_{n=1}^{\infty} \left[a_n(y) \cos n\omega \left(\frac{x}{2c_r} + t \right) + b_n(y) \sin n\omega \left(\frac{x}{2c_r} + t \right) \right] \sin \left(\frac{n\omega x}{2c_r} \right) \quad (3)$$

where $c_r = \beta c^2/f^2$ is the baroclinic Rossby wave speed and $x = 0$ is located at the ocean's eastern boundary. For $\gamma = \alpha\pi/L$ and the parameters appropriate for the tropical/subtropical wind gyres in the North Pacific, it can be shown that ignoring terms of $O(\gamma^3)$ and higher (which is equivalent to truncating the series expansion

at $n = 3$) results in less than 5% truncation error. In this case,

$$\begin{aligned} a_0 &= \frac{-x}{f\rho_0 c_r} \left[B(1 - \gamma^2) \sin \left(\frac{2\pi y}{L} \right) + \gamma A \cos(\omega\phi) \cos \left(\frac{2\pi y}{L} \right) \right], \\ a_1 &= \frac{-2}{f\rho_0 \omega} \left[2\gamma B \cos \left(\frac{2\pi y}{L} \right) + \left(1 - \frac{3\gamma^2}{2} \right) A \cos(\omega\phi) \sin \left(\frac{2\pi y}{L} \right) \right], \\ b_1 &= \frac{-2}{f\rho_0 \omega} \left(1 - \frac{\gamma^2}{2} \right) A \sin(\omega\phi) \sin \left(\frac{2\pi y}{L} \right), \\ a_2 &= \frac{1}{f\rho_0 \omega} \left[B\gamma^2 \sin \left(\frac{2\pi y}{L} \right) - \gamma A \cos(\omega\phi) \cos \left(\frac{2\pi y}{L} \right) \right], \\ b_2 &= \frac{1}{f\rho_0 \omega} A\gamma \cos(\omega\phi) \sin \left(\frac{2\pi y}{L} \right), \\ a_3 &= \frac{1}{3f\rho_0 \omega} A\gamma^2 \cos(\omega\phi) \sin \left(\frac{2\pi y}{L} \right), \\ b_3 &= \frac{1}{3f\rho_0 \omega} A\gamma^2 \sin(\omega\phi) \sin \left(\frac{2\pi y}{L} \right). \end{aligned} \quad (4)$$

Figure 4a gives an example of the h field calculated from (3) and (4); it has a pattern similar to the time-independent Sverdrup flow but with deviations caused by the baroclinic Rossby waves. Notice that as A and $\gamma \rightarrow 0$, the above solution reduces to the time-independent Sverdrup flow field.

If we neglect the detailed flow structures inside the western boundary, the mass conservation requires the inflow at the western boundary to bifurcate where $h = 0$ in Figure 4a. Although Rossby wave reflections can complicate the flow patterns near the western boundary, our model result in the next section (e.g., Figure 6) shows that the interior NEC near the bifurcation area moves rather smoothly into the Mindanao Current and the Kuroshio. This indicates that the distortion by the Rossby wave reflection may not be very important. Under this assumption we can derive the bifurcation latitude $Y_b(t)$ by solving $h(x, y, t) = 0$ for y at the western boundary $x = -W$. To the leading order of γ ,

$$Y_b(t) \simeq -\frac{\alpha A \cos(\omega\phi)}{2B} - \frac{2\alpha c_r}{\omega W} \sin \left(\frac{\omega W}{2c_r} \right) \cos \left(-\frac{\omega W}{2c_r} + \omega t \right). \quad (5)$$

The first term in (5) gives a constant offset for Y_b , due to the fact that the stronger wind stress curl occurs in winter when the zero wind-stress line shifts southward (see Figure 3). The second term determines the time dependency of the bifurcation latitude, and its amplitude depends on $2\alpha c_r/\omega W$ and $\sin(-\omega W/2c_r)$. In

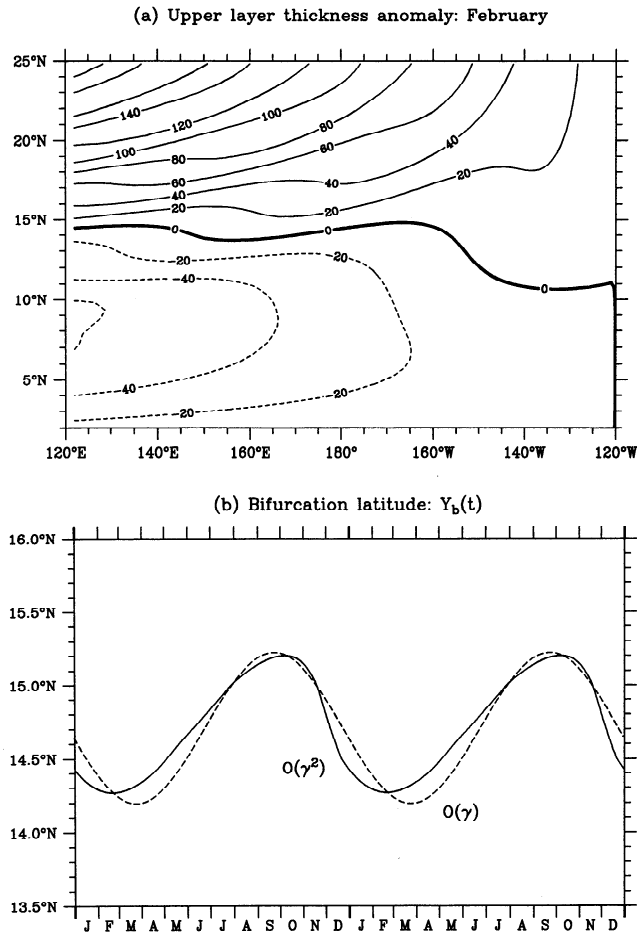


Figure 4. (a) Upper layer thickness anomaly pattern (in February) derived from the time-dependent Sverdrup theory. Contour unit is meters. (b) Annual migration of the NEC's bifurcation latitude. The dashed line gives the result predicted by (5), in which only the annual Rossby wave is considered. The solid line is calculated from (3) and (4), with terms up to $n = 3$ retained. For clarity, the annual cycle is plotted for 2 years.

$\sin(-\omega W/2c_r)$ the parameter $\omega W/2c_r$ represents the phase when the interface displacement at the center of mass of the wind stress curl field (in this case at $-W/2$) reaches the western boundary at the baroclinic Rossby wave speed. If $\omega W/2c_r = k\pi$ with k being an integer, Y_b becomes time-independent. For values appropriate along the bifurcation latitude of the North Pacific ($\omega = 1.99 \times 10^{-7} \text{ s}^{-1}$, $W = 1.20 \times 10^7 \text{ m}$, and $c_r = 0.16 \text{ m s}^{-1}$), $\sin(\omega W/2c_r) = 0.94$, suggesting that the western boundary exists near an antinodal point and that a maximum annual migration of the bifurcation point may be expected.

Figure 4b shows the migration of Y_b as a function of time. The dashed line is the result according to (5), i.e., when only the annual Rossby wave effect is considered. The solid line shows the result when the next higher-order corrections are included. Notice that Y_b reaches the northernmost position in October and the south-

ernmost position in February. The swifter southward migration, as indicated by the solid line in Figure 4, is due to the excitation of subharmonics of the annual Rossby waves. Although the western boundary exists near an antinodal point, the amplitude of the Y_b migration is about 1° latitude, which is only $1/9$ that of the surface wind stress curl system. This small migration is due to the relatively small value of $2c_r/\omega W (= 0.13)$ in (5). In other words, near the NEC's bifurcation latitude it takes the annual Rossby waves longer than 1 year to reach the western boundary. Physically, the small migration can be understood as follows: as the zero wind stress curl line shifts northward, the positive wind stress curl anomaly deepens the upper layer thickness and tends to force Y_b northward when its influence reaches the western boundary. Before the signals in the east can reach the western boundary, however, the seasonal wind changes its phase and the negative height anomalies created in the west now tend to force Y_b southward. This cancels the effectiveness of shifting the bifurcation latitude by the seasonally migrating wind system.

Notice that the amplitude of the migration of Y_b is not only proportional to α (the excursion amplitude of the zero wind stress curl line), but also it depends on the forcing frequencies. As indicated by (5), for lower-frequency wind fluctuations (with smaller ω) the bifurcation latitude may migrate at a larger amplitude. Physically, less phase cancellation will take place as ω becomes smaller.

Numerical Model and Its Verification

Although the above linear model provided some insights into the bifurcation of the NEC, especially its dependence upon the basin-scale wind fluctuations, the NMK current system exists close to the western boundary where nonlinear dynamics can possibly alter the ocean circulation patterns presented in section 2. Also, realistic wind forcing can further complicate the results. As we noted in the Introduction, many previous investigators have successfully used linear and nonlinear reduced-gravity models to reproduce features of seasonal and interannual variability in the low-latitude Pacific Ocean. In this study we will use the nonlinear version of the reduced-gravity model and focus our attention on the region of the NMK system.

Equations that govern the upper ocean motion in a reduced-gravity system (i.e., assuming the deep layer is inert) can be written as follows:

$$\frac{\partial u}{\partial t} - \zeta v H = -\frac{\partial E}{\partial x} + A_h \nabla_h^2 u + \frac{\tau^x}{\rho_o H} \quad (6)$$

$$\frac{\partial v}{\partial t} + \zeta u H = -\frac{\partial E}{\partial y} + A_h \nabla_h^2 v + \frac{\tau^y}{\rho_o H} \quad (7)$$

$$\frac{\partial H}{\partial t} + \frac{\partial(uH)}{\partial x} + \frac{\partial(vH)}{\partial y} = 0 \quad (8)$$

where

$$\zeta = \frac{1}{H} \left(f + \frac{\partial v}{\partial x} - \frac{\partial u}{\partial y} \right), \quad E = g'H + \frac{1}{2}(u^2 + v^2).$$

In the above equations, (u, v) are the velocity components in the (x, y) directions, H is the thickness of the upper layer, ∇_h^2 is the horizontal Laplacian operator, A_h is the coefficient of the horizontal eddy viscosity coefficient, ρ_o is the reference water density, and (τ^x, τ^y) are the x and y components of the surface wind stresses, respectively.

Figure 5 shows the model domain and the grid point distribution used in this study. To focus on the NMK system, the grid has the finest resolution of $1/7^\circ$ latitude by $1/7^\circ$ longitude near the Philippine coast. The grid size decreases gradually away from the western boundary to $1/2^\circ$ in latitude and 1° in longitude. The model domain is bounded by land to the east and west. Meridionally, it extends from 15°S to 38°N , encompassing the entire tropical and subtropical gyres in the North Pacific and the whole tropical gyre in the South Pacific.

Equations (6)–(8) are solved in finite difference form by using the energy-conserving scheme proposed by Sadourney [1975]. Arakawa's C grid is used in defin-

ing the staggered positions for the dependent variables u , v , and H [Arakawa and Lamb, 1977]. Along the model's open boundaries, no-normal flow and free-slip conditions are used. No-normal flow and nonslip conditions are used along the coast or marginal seas (depth < 200 m). Following Inoue and Welsh [1993], the mean upper layer thickness of the model is set to 300 m and g' is chosen to be 0.035 m s^{-2} . The horizontal eddy viscosity coefficient is $500 \text{ m}^2\text{s}^{-1}$ for the whole model domain, except near the northern boundary where A_h is increased linearly to $1500 \text{ m}^2\text{s}^{-1}$ from 30°N to 38°N . The increased A_h value is used to suppress instabilities occurring in the Kuroshio/Kuroshio Extension regions and to damp spurious coastal Kelvin waves along the artificial northern boundary.

The model ocean, which is initially at rest, is first spun up by the climatological FSU wind for 20 years until the quasi steady state is reached. It is then forced by the monthly FSU wind [Goldenberg and O'Brien, 1981] for the 32 years from January 1961 through December 1992. The pseudo-stress values of FSU were converted to the surface wind stresses by using a drag coefficient of 1.5×10^{-3} . In regions where monthly FSU wind data are not available (i.e., north of 30°N and west of 124°E), we used the climatological, Hellerman and Rosenstein

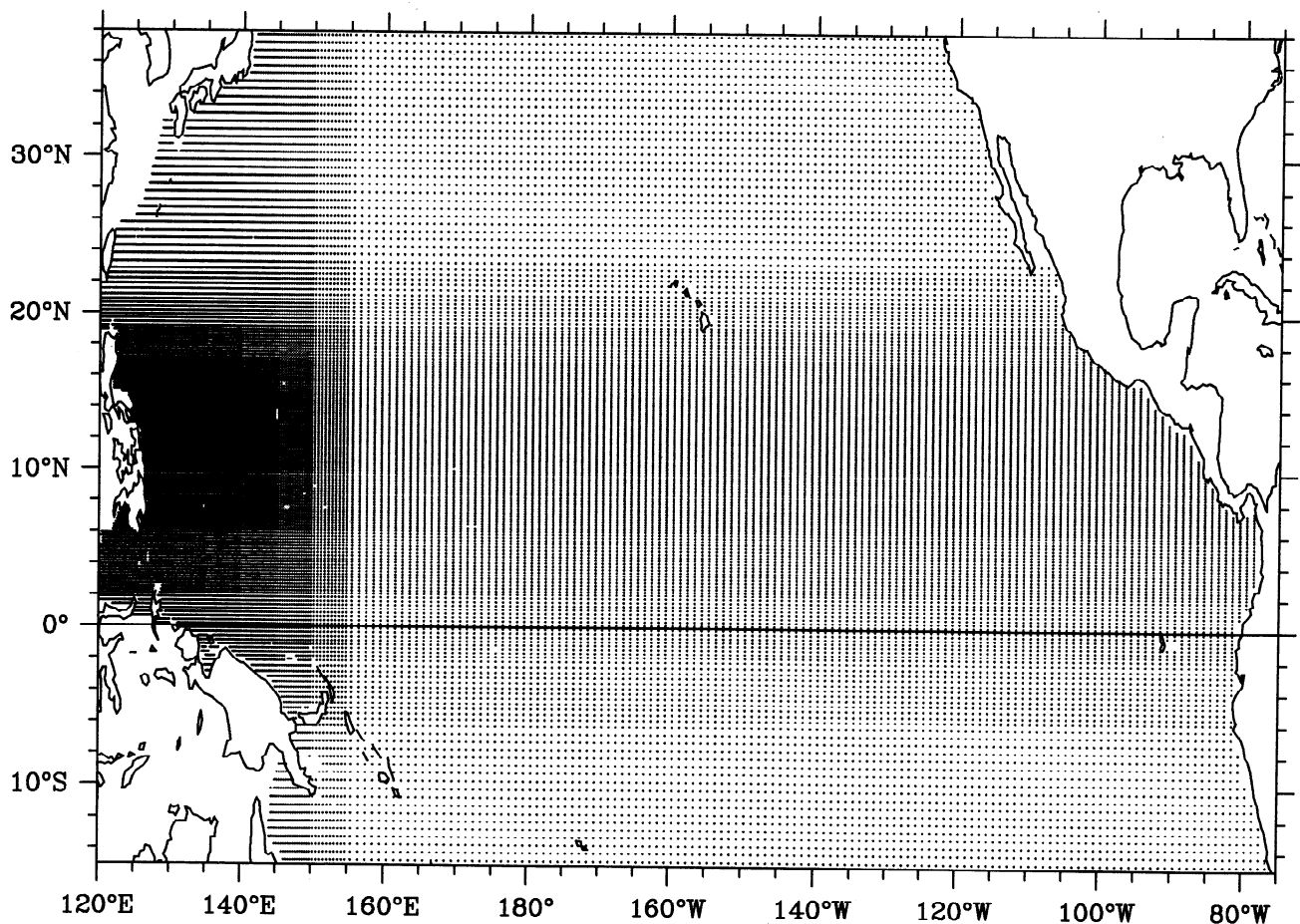


Figure 5. Grid point distribution for the nonlinear, reduced-gravity model. The grid points are denoted with dots, and the finest resolution near the Philippine coast is $1/7^\circ \times 1/7^\circ$.

[1983] monthly wind data instead. Because the inter-annual changes in the NEC near the western boundary are largely determined by the surface wind fluctuations south of 30°N (see *Qiu and Joyce* [1992] for the analysis along 137°E), we expect that this use of the climatological data north of 30°N is acceptable for our study on the NMK current system.

Figure 6 shows typical upper layer thickness and velocity patterns in the region of the NMK system simulated from the present model. The general picture of the NEC's bifurcation into the Kuroshio and the Mindanao Current along the Philippine coast agrees with the classical picture presented in Figure 1. Notice that other modeled features, such as quasi-stationary meanders of the North Equatorial Countercurrent (NECC) and intrusions of the Mindanao Current into the Celebes Sea, also compare favorably with the in-situ measurements reported by *Lukas et al.* (1991).

A more stringent check of our multiyear simulation is to compare the modeled sea level changes (i.e., $\Delta\rho H/\rho_0$)

with those measured from in-situ sea level stations. To do so, we have chosen three representative stations, among which, Malakal is located offshore of the Mindanao Current, Guam in the westward flowing NEC, and Chuuk in the eastward flowing NECC (see Figure 6a for locations of the sea level stations). Figure 7 shows the time series of the 5-day-averaged sea level anomalies from the in-situ observations (solid lines) and the model simulation (dashed lines). Generally good agreement exists between the sea level fluctuations from the in-situ observations and from the model on timescales longer than seasons. Linear regression estimations reveal that the correlation coefficients between the time series of the model and observations are 0.43 (for Malakal), 0.51 (Guam), and 0.43 (Chuuk), respectively. Though low in magnitude, for the estimated 22 degrees of freedom in the time series, all these values are significant at the 95% confidence level.

On the intraseasonal timescale the power spectra of the modeled sea level at Malakal and Chuuk have a higher energy level than those of the observations. At Guam the observed and modeled energy levels agree reasonably well. This suggests that the eddies associated with the NECC in the model are possibly too energetic. On a monthly timescale or less the modeled sea level generally has a smaller rms amplitude than the observations due to the use of monthly averaged wind data. Despite these problems and the simplicity of the assumed model physics, our present multiyear model run is successful in simulating the upper ocean changes of the NMK system on a timescale longer than seasons. In the following sections the 5-day-averaged model results from 1961 through 1992 will be analyzed to clarify the variability and its causes in the NMK system.

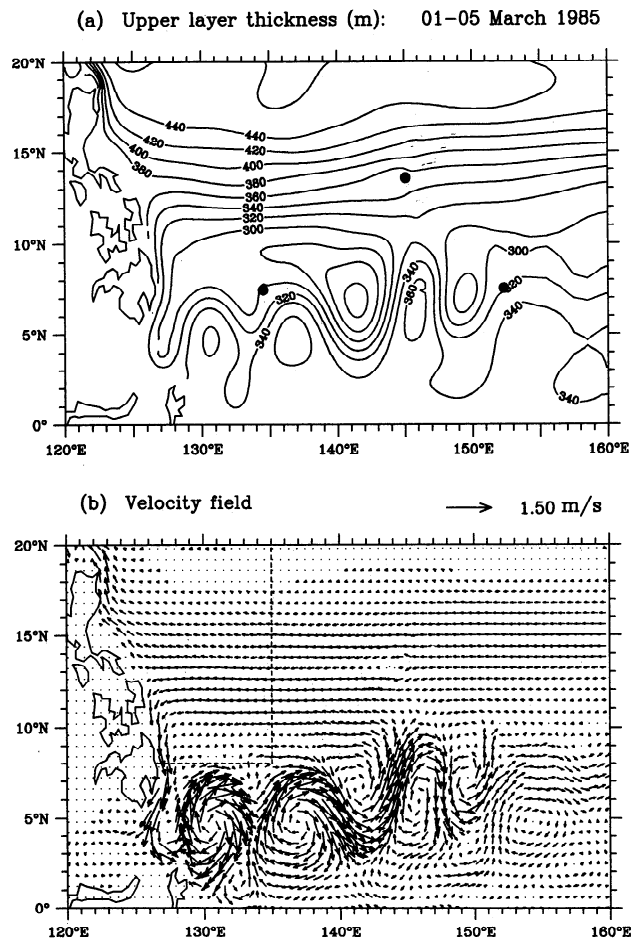


Figure 6. Example of (a) the upper layer thickness and (b) the horizontal velocity field obtained from the nonlinear, reduced-gravity model. Solid dots in Figure 6a denote the sea level stations of Malakal (134.47°E, 7.33°N), Guam (144.65°E, 13.43°N), and Chuuk (151.85°E, 7.45°N). The dashed line in Figure 6b denotes the NMK area through which the transport fluctuations are considered.

Meridional Fluctuations of the NEC's Bifurcation

First, we will focus on the changes in the bifurcation latitude Y_b of the NEC. From the model output we define Y_b to be where the meridional velocity component averaged within the 2° band along the western boundary is zero. In the case shown in Figure 6b, for example, the NEC bifurcates at 13.0°N. Choosing other widths for averaging is found to have little effect on the resultant Y_b time series. Figure 8 shows the time series of the model-derived Y_b from 1961 through 1992. The seasonal signals with characteristics similar to those found in Figure 4 are discernible in Figure 8, namely, Y_b tends to migrate northward in the spring and summer seasons and tends to retreat southward in winter.

In addition to the seasonal signals, interannual changes in Y_b are also clear in Figure 8. In order to separate the interannual signals from the seasonal ones, we conducted a companion model run in which we forced the model ocean using the FSU climatological monthly wind data (averaged over 1961-1992). Because of non-linearity, the model's flow patterns are slightly different

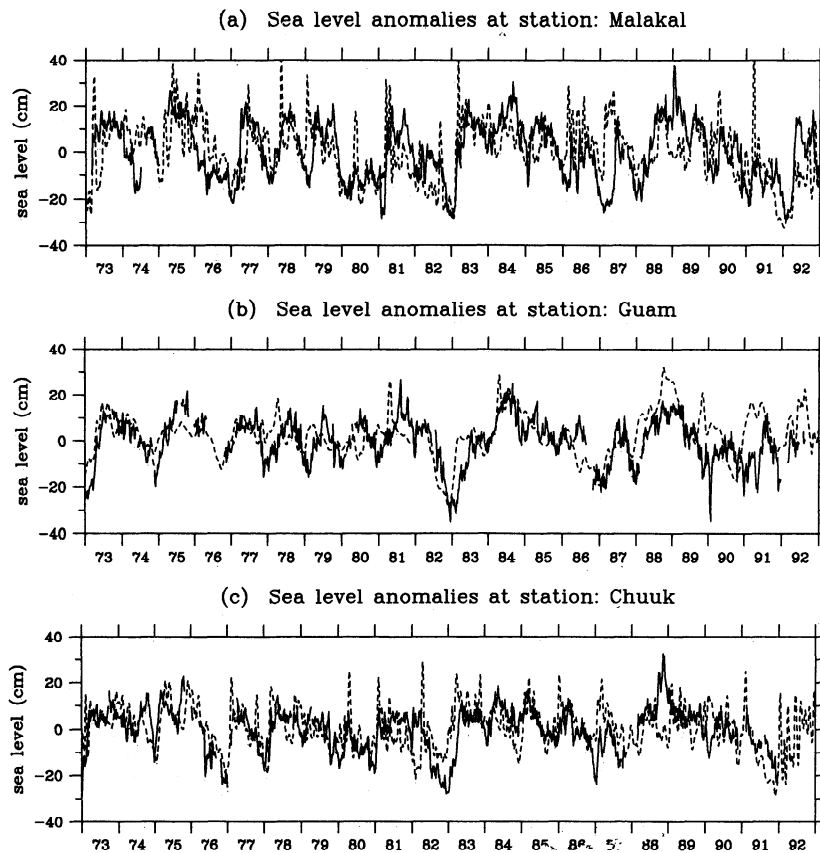


Figure 7. Comparisons between the in-situ observed sea level anomalies (solid lines) and the model-simulated sea level anomalies (dashed lines) at stations (a) Malakal, (b) Guam, and (c) Chuuk. All values are 5-day averages without further low-pass filtering applied. See Figure 6a for locations of the three sea level stations.

from 1 year to another. Figure 9 shows the seasonal migration of the bifurcation latitude averaged over the 10-year model run. While the phase of Y_b agrees with the result from the linear model, the amplitude of Y_b from the nonlinear model is about 2.5 times as large as that obtained from the linear model (Figure 4). Notice that the differences between Figures 4 and 9 are

largely due to the fact that the observed, monthly wind stress curl pattern over the Pacific is not strictly zonal as is assumed in the linear model. For example, in the months of October and November the NEC's bifurcation in the nonlinear model occurs at a latitude considerably more north than it does in the linear model. This large northward shift is due to the southwest Asian

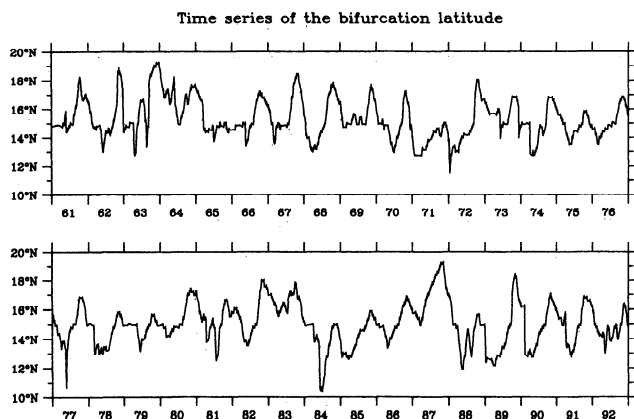


Figure 8. Time series of the bifurcation latitude Y_b from the nonlinear model driven by the FSU monthly wind data (1961–1992). Here Y_b is defined as where the meridional velocity component averaged within the 2° band along the western boundary is zero.

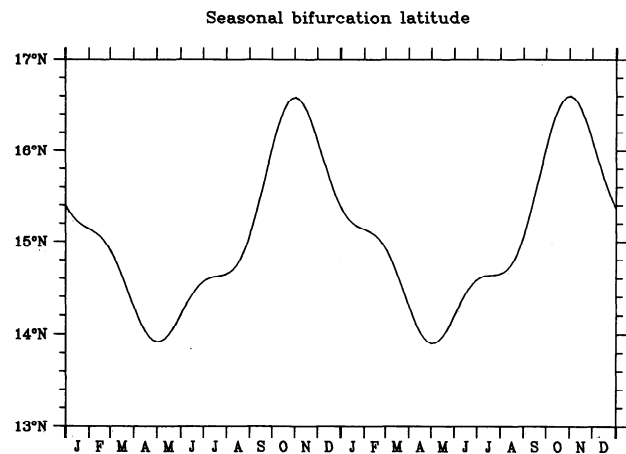


Figure 9. Bifurcation latitude as a function of months from the nonlinear model run that is driven by the climatological monthly wind data. The monthly values are averages from the 10-year model run.

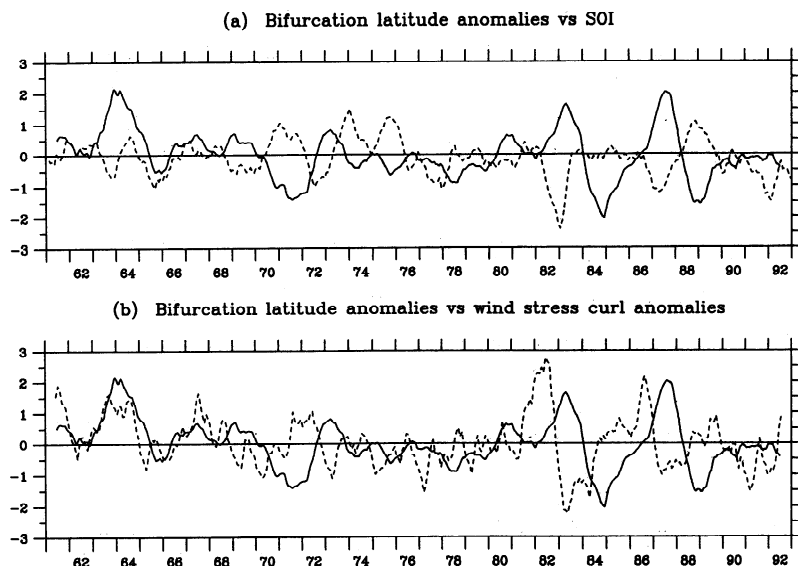


Figure 10. (a) Time series of the NEC's bifurcation latitude anomalies (solid line) versus the southern oscillation index (SOI) (dashed line). The solid line is derived by applying a 12-month running-mean filter on the time series shown in Figure 8 and by removing the mean. The ordinate unit is degrees for the bifurcation latitude anomalies and 2.5 hPa for the SOI. (b) Time series of the NEC's bifurcation latitude anomalies (solid line) versus the wind stress curl anomalies averaged in the zonal band of 12°–18°N (dashed line). The curl anomalies are computed from the FSU monthly wind data with a 12-month running-mean filter applied. The ordinate unit for the wind stress curl is 10^{-8} N m^{-3} .

monsoon whose presence curves the zero wind stress curl line northward in the western Pacific (see Figure 2b). Because of their proximity to the bifurcation area, the positive wind stress curl anomalies (from the zonal average) work to shift Y_b to a more northerly latitude.

To focus on the interannual changes in the bifurcation latitude, we show in Figure 10a the time series of Y_b after applying a 12-month, running-mean filter and removing the mean (see the solid line). Large-amplitude and positive anomalies are most prominent in years 1963/1964, 1982/1983, and 1987, but they also can be seen in 1969 and 1972/1973. As indicated by the superimposed southern oscillation index (SOI) (Figure 10a, dashed line), all of these peaks followed the mature phase of the warm episodes of the El Niño–Southern Oscillation. Many of the large-amplitude, negative Y_b anomalies (1971, 1974, and 1988/1989), on the other hand, followed the cold phases of the ENSO. Because of the large-scale nature of the ENSO events, it is natural to seek causes for these interannual changes in Y_b in the basin-scale wind field. To do so, we examined the interannual changes in the wind stress curl field averaged in the zonal band between 12°N and 18°N across the Pacific Ocean (see Figure 10b, dashed line). As can be seen from the wind stress curl maps shown in Figure 2, a positive anomaly of this value occurs either when the zero wind stress curl line moves to a more northerly latitude or when the positive wind stress curl of the tropical wind gyre intensifies. Both of these situations are likely to cause the NEC to bifurcate at a higher latitude. By overlaying the Y_b time series on Figure 10b,

we note that there is indeed a good correspondence between the positive Y_b anomalies and the positive wind stress curl anomalies, with the latter preceding the former by about a year.

Figure 11 gives a more quantitative comparison of the wind stress curl anomalies with the SOI and the Y_b anomalies. The dashed line, showing the cross-

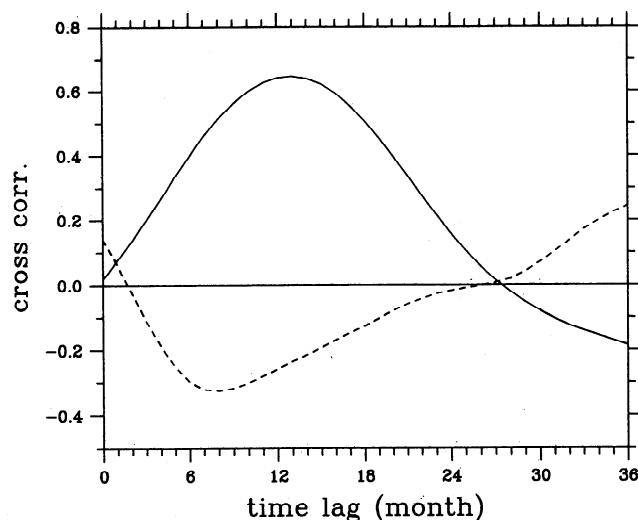


Figure 11. Cross correlation of the wind stress curl anomalies in the zonal band of 12°–18°N with the bifurcation latitude anomalies (solid line) and with the SOI (dashed line). The x axis denotes the lag of the Y_b anomalies or the SOI behind the wind stress curl anomalies.

correlation coefficients with the SOI, reveals that the wind stress curl in the zonal band of 12°–18°N tends to increase prior to the mature phase of ENSO events. The correlation reaches a negative peak when the SOI lags 7 months behind the wind stress curl anomalies.

The cross correlation between the anomalies of the wind stress curl and Y_b has a relatively wide band of positive coefficients centered around the 13-month time lag (Figure 11, solid line). The appearance of this wide band, instead of a maximum at a narrowly defined time lag, is no surprise: during each ENSO event the center of the wind stress curl anomalies is located at a different longitude. As we found in (5), a wind stress curl anomaly will induce a maximum response in Y_b when its center of mass reaches the western boundary at the speed of the long, baroclinic Rossby wave. With the positions of the positive wind stress curl anomalies at various longitudes during different ENSO events, the responses in Y_b lag differently, resulting in the wide band of the cross correlation shown in Figure 11. Notice that a 13-month time lag places the center of mass of the wind stress curl anomalies near the date line. This result is congruent with the analysis of the FSU data by Kessler [1990], who showed that the interannual variability in the zonal component of the surface wind stress has its maximum amplitude around the date line (see Kessler, 1990, Figure 17).

Transport Fluctuations in the NMK Current System

In order to quantify the transport fluctuations of the NMK system, we examined the mass fluxes through the area from 8°N to 20°N and from the coast of the Philippines to 135°E (referred to hereinafter as the NMK area; see the dashed line in Figure 6b). We define the transports for the NEC, the Mindanao Current, and the Kuroshio by

$$\begin{aligned} T_{\text{NEC}} &= - \int_{8^{\circ}\text{N}}^{20^{\circ}\text{N}} (uH) dy && \text{along } 135^{\circ}\text{E}, \\ T_{\text{MC}} &= - \int_{126^{\circ}\text{E}}^{135^{\circ}\text{E}} (vH) dx && \text{along } 8^{\circ}\text{N}, \\ T_{\text{KC}} &= + \int_{120^{\circ}\text{E}}^{135^{\circ}\text{E}} (vH) dx && \text{along } 20^{\circ}\text{N}, \end{aligned} \quad (9)$$

respectively. The signs here are chosen such that the three currents have nominally positive transport values. Because the NMK area is enclosed, $T_{\text{NEC}} \simeq T_{\text{MC}} + T_{\text{KC}}$, and only relatively weak mass convergence/divergence with a rms amplitude of 5.1 Sv occurs due to transient motions. For transport fluctuations with annual and interannual frequencies, T_{NEC} is nearly always balanced by the sum of T_{MC} and T_{KC} .

Figure 12 shows the time series and their respective power spectral density distributions of T_{NEC} , T_{MC} , and T_{KC} from the 5-day-averaged model output. The

high-frequency, intraseasonal fluctuations seen in T_{NEC} and T_{MC} are caused by the anticyclonic meanders of the NECC (see Figure 6b). As they develop and pass through the southeastern corner of the NMK area, these meanders can significantly lower the transports of the NEC and the Mindanao Current. This influence of the NECC's anticyclonic meander upon the transports of the NEC and the Mindanao Current is also evident in the observations reported by *Wijffels et al.* [1995, Table 1]: during one of the cruises they found the southward transport of the Mindanao Current reduced to zero due to the appearance of an anticyclonic eddy passing through the NMK area. Because the occurrence of these meanders is intraseasonal, it is not surprising, as we depict in Figure 13a, that the fluctuations in T_{NEC} and T_{MC} with frequencies higher than 1 cycle per year (cpy) are essentially coherent. Notice that in the power spectral density distributions for the NEC and the Mindanao Current, the spectral slope, with frequencies less than 6 cpy, is $\sim \omega^{-1}$ and there exists a sharp drop in energy in the higher-frequency band. This energy drop is due to the use of monthly wind data to drive the model. In the transport fluctuations of the northward flowing Kuroshio, little energy is found to exist in the intraseasonal frequency band (Figure 12c). This lack of energy is partially due to the absence of a return flow, like the NECC, at the latitude of 20°N and partially due to the fact that coastal Kelvin waves propagate southward along the western boundary, which tends to transfer incident disturbances preferentially into the southward flowing Mindanao Current.

For the seasonal transport fluctuations ($\omega = 1$ cpy), Figure 12 indicates that the spectral peaks are more prominent in T_{MC} and T_{KC} than in T_{NEC} . Moreover, the seasonal transport fluctuations between the NEC and the Kuroshio are nearly in-phase ($\sim \pi/4$, Figure 13b), whereas they are about $3\pi/4$ out of phase between the NEC and the Mindanao Current (Figure 13a). In Table 1 we summarize the bimonthly T_{NEC} , T_{MC} , and T_{KC} values from the 32-year model simulation. It is worth emphasizing that these same seasonal signals were noted by *Wyrтки* [1961]; using data from available ship observations near the NMK area, he showed that no clear seasonal signals exist in the inflow NEC and that the baroclinic transport of the Kuroshio has a seasonal maximum in spring and fluctuates out of phase with that of the Mindanao Current. Lack of the annual signal in the NEC near the western part of the North Pacific was also noted by *Kessler* [1990] in his analysis of expendable bathythermograph (XBT) data.

Some insights into these observed seasonal signals can be obtained from the analytical model results presented in section 2. In the time-dependent Sverdrup model the seasonal anomalies in T_{KC} across the northern boundary of the NMK area are proportional to $h(x, y, t)$ at $x = 135^{\circ}\text{E}$ and $y = 20^{\circ}\text{N}$, where h is the upper layer thickness anomaly (recall (3)). Similarly, the seasonal anomalies in T_{MC} across the southern boundary of the

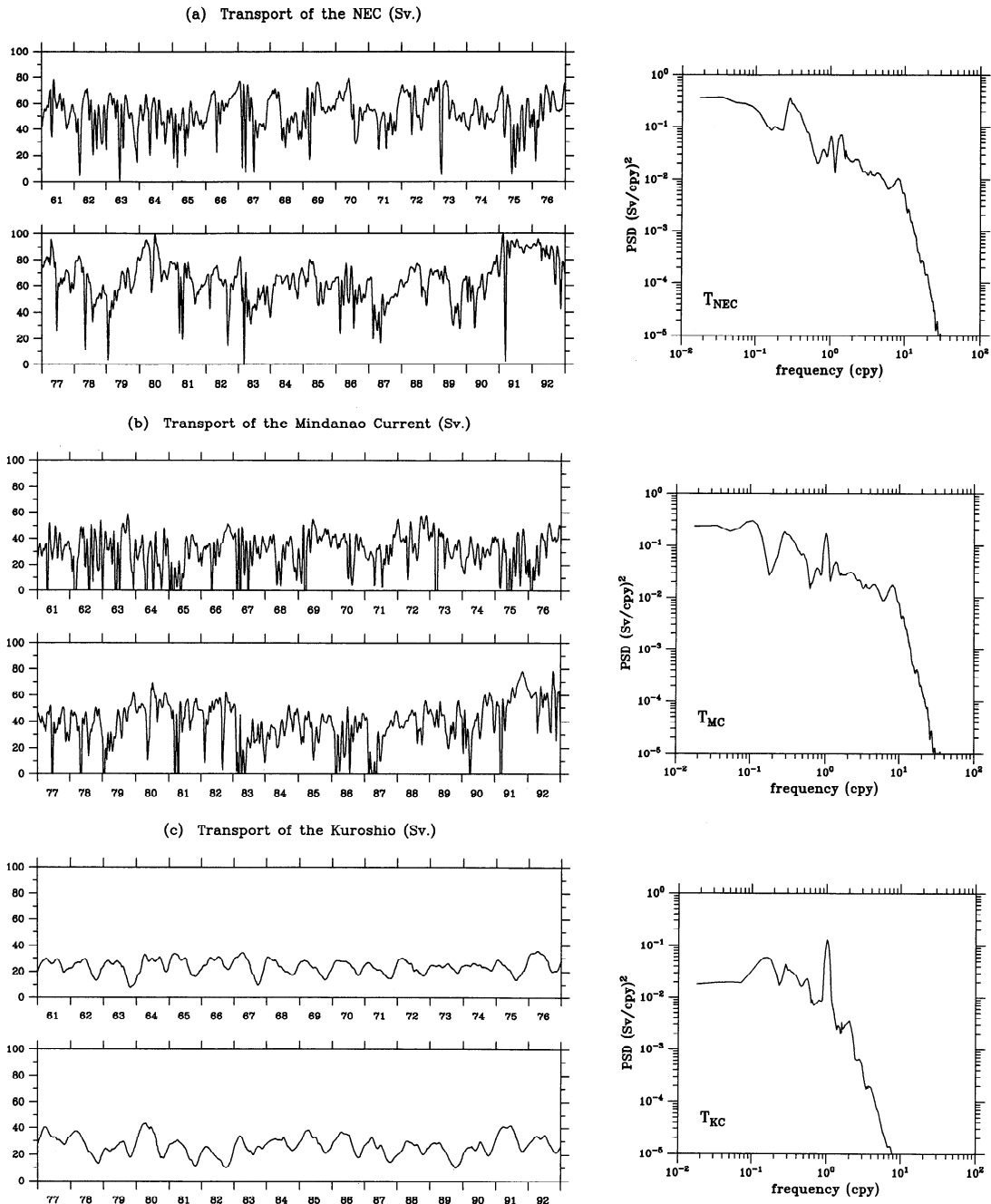


Figure 12. Time series and their power spectral density distributions of (a) the NEC through the eastern boundary of the NMK area, (b) the Mindanao Current through the southern boundary of the NMK area, and (c) the Kuroshio through the northern boundary of the NMK area. Here the transport values are calculated from the 5-day-averaged model output, and the NMK area is defined by the dashed line shown in Figure 6b.

NMK area are proportional to $-h(x, y, t)$ at $x = 135^\circ\text{E}$ and $y = 8^\circ\text{N}$. As we discussed in section 2, the critical parameter for the seasonally varying $h(-W, y, t)$ field is $\omega W/2c_r$. For values appropriate for the 20°N latitude of the Pacific, $\omega W/2c_r \simeq 4.3\pi$; this suggests that the seasonal anomalies in T_{KC} will have a maximum in spring and a minimum in fall. On the other hand, $\omega W/2c_r \simeq 0.8\pi$ for the $-h(x, y, t)$ field at $x = 135^\circ\text{E}$ and $y = 8^\circ\text{N}$ and the seasonal anomalies in T_{MC} will be about 180° out of phase with those in T_{KC} . Because

the T_{KC} anomalies are about 180° out of phase with the T_{MC} anomalies, the seasonal anomalies in T_{NEC} , which are the sum of T_{KC} and T_{MC} , tend to have an amplitude smaller than either of the T_{MC} and T_{KC} anomalies. This argument gives a simple explanation for the observed seasonal cycle in the NMK current system presented by *Wyrtki* [1961] and *Kessler* [1990].

To examine the transport fluctuations in the interannual frequency band, we low-pass filtered the time series of Figure 12 and removed the fluctuations with frequen-

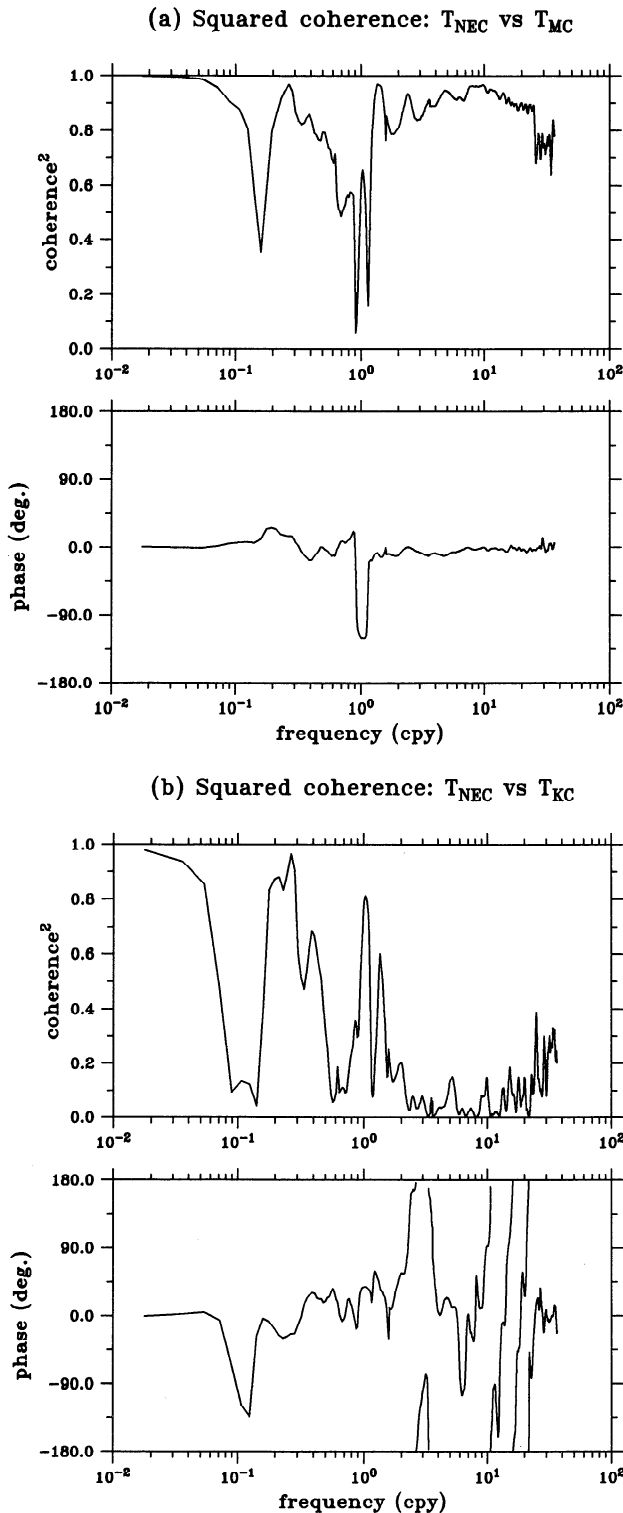


Figure 13. Squared coherence amplitude and phase between the transport time series of (a) the NEC and the Mindanao Current (see Figures 12a and 12b) and (b) the NEC and the Kuroshio (Figures 12a and 12c).

cies higher than 0.9 cpy. As shown in Figure 14, the low-pass-filtered time series of T_{NEC} and T_{MC} are dominated by the signals with periods of 2–5 years, a result also identifiable from the power spectral density distributions of Figures 12a and 12b. It is useful here to discuss

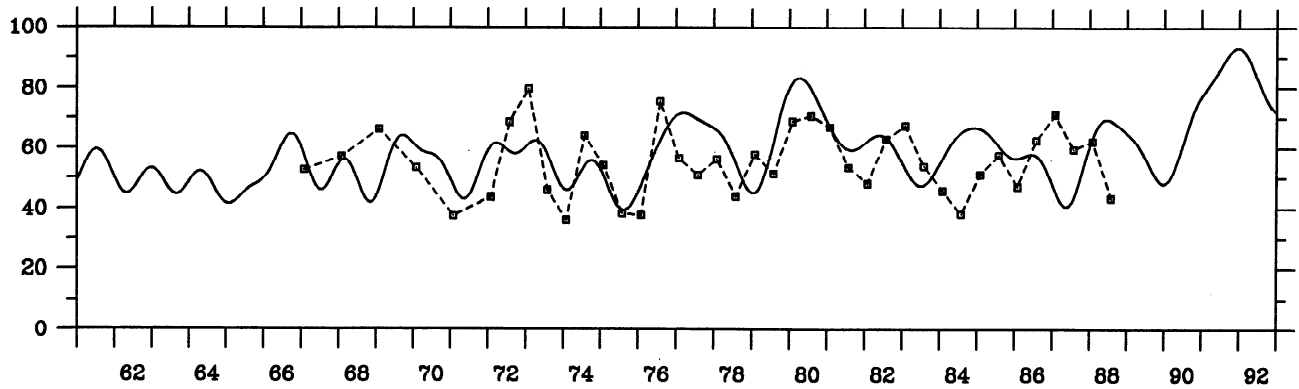
these interannual transport changes through comparisons with available in-situ observations. For the NEC's transport in the western Pacific the Japan Meteorological Agency has carried out repeated hydrographic surveys since 1967 along the 137°E meridian. Using the hydrographic data from the 39 cruises of 1967–1988, *Qiu and Joyce* [1992] extracted the interannual fluctuations of the NEC's transport through an empirical orthogonal function analysis. Figure 14a (squares) shows the transport values of T_{NEC} derived from their analysis. Despite the fact that the repeat hydrographic data are subject to aliasing by strong eddies in the NECC, the modeled time series seems to compare favorably with that derived from the in-situ observations, especially prior to 1984. Many of the transport peaks in Figure 14a concurred with the mature phase of the El Niño events in the eastern tropical Pacific, e.g., 1969, 1972, 1976, 1982/1983, 1986/1987, and 1991/1992 (see the SOI in Figure 10a). Notice that not all the T_{NEC} peaks in Figure 14a correspond to the ENSO events. In 1980, for example, while there was no indication of a warm episode in the eastern tropical Pacific, a strong intensification of the NEC is found both in the model and in the observations (see *Donguy et al.* [1982] for the other “ENSO-like” signals observed in the western Pacific in 1980). This increase in T_{NEC} is due to the presence of the quasi-biennial fluctuations in the surface wind stress curl field in the western low-latitude Pacific (see discussion below). Although these quasi-biennial wind forcings are phase locked with the ENSO events, some of their effects are confined to the western part of the low-latitude Pacific and do not lead to the warming of the eastern equatorial Pacific.

Interannual fluctuations in the Mindanao Current have been previously studied by *Lukas* [1988] using the sea level records from the Malakal and Davao tide gauges. In particular, *Lukas* emphasized the presence of the quasi-biennial oscillations in the sea level difference between Davao and Malakal, which can be regarded as an indicator for T_{MC} , assuming a constant mean upper layer thickness. The time series of the sea level difference of Davao minus Malakal is shown in Figure 14b (dashed line). To compare with the model result, we have used the monthly mean sea level data and converted the sea level difference to the transport anomaly

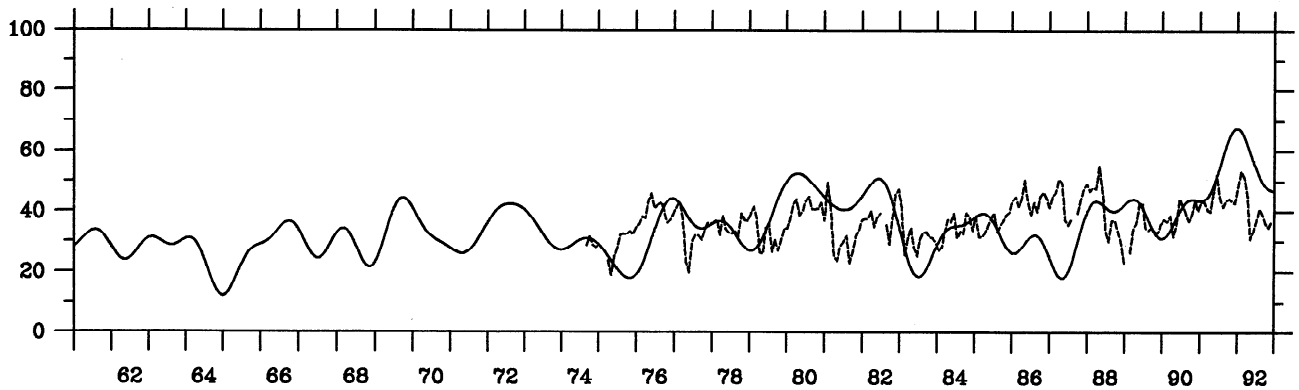
Table 1. Transport Values for the North Equatorial Current, the Mindanao Current, and the Kuroshio Through the NMK Area (120°E–135°E, 8°N–20°N)

Time	T_{NEC}	T_{MC}	T_{KC}
Jan. – Feb.	59.0	27.8	28.3
March – April	59.9	26.6	30.2
May – June	57.9	29.0	28.0
July – Aug.	54.9	32.3	24.6
Sept. – Oct.	53.3	36.4	19.2
Nov. – Dec.	55.9	35.7	21.5
Annual	56.8	31.4	25.4

(a) Low-pass filtered NEC transport (Sv.)



(b) Low-pass filtered Mindanao Current transport (Sv.)



(c) Low-pass filtered Kuroshio transport (Sv.)

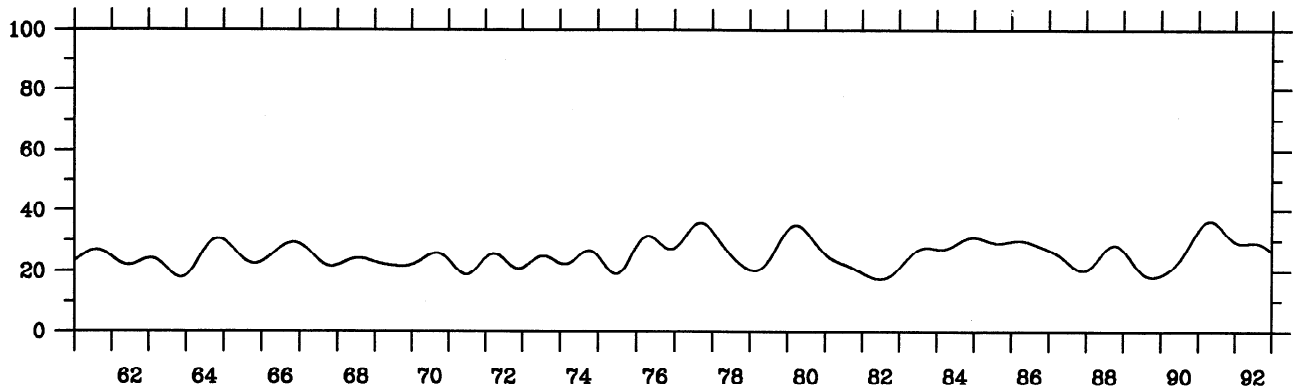


Figure 14. Interannual fluctuations in the transports of (a) the NEC, (b) the Mindanao Current, and (c) the Kuroshio. The solid lines are the model results after filtering out signals with frequencies >0.9 cpy. The squares in Figure 14a denote the filtered NEC transports estimated from hydrographic observations along 137°E from 8°N to 12°N . The dashed line in Figure 14b denotes the interannual changes in the Mindanao Current inferred from the low-pass-filtered sea level differences of Davao minus Malakal.

at a rate of $8.3 \text{ Sv per } 10 \text{ cm}$ [Lukas, 1988]. The quasi-biennial fluctuations, which are particularly prominent in the sea level data from 1975 to 1984, are also discernible in the modeled T_{MC} time series. The model simulation failed to reproduce the transport fluctuations for the period of 1986-1989, although it did hind-cast the increase in 1991. The discrepancies can be due

to the uncertainties in the surface wind field; they may also be induced by assuming a constant upper layer for converting the sea level difference to T_{MC} .

Continuous observations of the Kuroshio east of the Philippines are unfortunately not available, thus preventing us from comparing the modeled time series (Figure 14c) with in-situ measurements. Although the mag-

nitude of the interannual changes in T_{KC} is small relative to the NEC and the Mindanao Current, Figure 13b shows that the T_{KC} fluctuations on timescales of 3–7 years are coherent with the T_{NEC} fluctuations. In the quasi-biennial frequency band, Figure 13 reveals that the coherence between the transports of the Kuroshio and the NEC is considerably lower (< 0.4) than that between the Mindanao Current and the NEC (≈ 0.8). Since the interannual changes in T_{NEC} are dominated by the basin-scale wind stress curl anomalies, one possibility for this difference is that the quasi-biennial anomalies in the surface wind field are confined to the tropical gyre of the North Pacific, so that they are less effective in bringing about changes in the northward flowing Kuroshio. To test this hypothesis, we decomposed the FSU wind stress curl data (1961–1992) in the frequency domain. Figures 15a and 15b show the rms amplitudes of the wind stress curl in the quasi-biennial ($1.8 < \text{period} < 2.2$ years) and ENSO ($3 < \text{period} < 7$ years) frequency bands, respectively. Compared with the ENSO component, it is clear that the quasi-biennial component of the wind stress curl field has less variance in the subtropical region of the North Pacific. This result is

in accordance with our hypothesis that the interannual fluctuations with the ENSO timescale are likely to be detected in the Kuroshio, whereas those with the quasi-biennial timescale are only noticeable in the southern limb of the NMK system. Several recent studies have suggested that the ocean-atmosphere-land interaction in the low-latitude western Pacific is likely to allow the alternating strong and weak Asian monsoons, resulting in the regional quasi-biennial oscillations in the surface wind field [e.g., Meehl, 1987; Yasunari, 1989; Barnett, 1991; Masumoto and Yamagata, 1991].

Conclusions

In this study we investigated, in detail, the seasonal and interannual fluctuations in the NEC-Mindanao Current-Kuroshio system near the Philippine coast. Since the principal external forcing for the upper ocean changes is the surface wind, foci of this study have been on how the large-scale, low-frequency wind changes influence the bifurcation of the NEC and their consequences for the transport fluctuations in the Kuroshio and the Mindanao Current.

On the seasonal timescale the zonally averaged zero wind stress curl line over the North Pacific migrates from 11°N in late winter to 20°N in fall. As this large-scale wind system migrates in time, it induces upper layer thickness anomalies across the Pacific basin. Because the anomalies from different longitudes arrive at the western boundary at different phases of the seasonal cycle, their integral effect upon the NEC's bifurcation tends to be small due to phase cancellation. Using values appropriate for the NEC, we found that the latitudinal excursion of the bifurcation latitude due to the zonally averaged wind stress curl is only about 110 km, from 14°N to 15°N . This excursion is considerably smaller than the 1000-km migration in the seasonal wind stress curl field. The deviation from the zonal mean wind stress curl field, which is particularly important along the western boundary in September and October when the southwest Asian monsoon prevails, is, on the other hand, effective in changing the NEC's bifurcation latitude. With its anomalous positive wind stress curl along the Philippine coast the southwest monsoon tends to shift Y_b to a higher latitude ($\sim 16.5^\circ\text{N}$) in October and November.

The bifurcation latitude of the NEC is further found to be susceptible to the interannual changes of the surface wind. Prior to the mature phases of El Niño, we found that the positive wind stress curl field in the northeast trade wind belt (12° – 18°N) tends to intensify, causing the NEC to subsequently bifurcate at a higher latitude. Depending on the longitude of the center location of the wind stress curl anomalies, the response of the bifurcation to each ENSO event can differ. The northernmost excursion of Y_b usually occurs about a year after the mature phase of ENSO events, as most of the wind stress curl anomalies are centered near the date line. The excursion amplitude can reach as large as 2 – 3° in latitude.

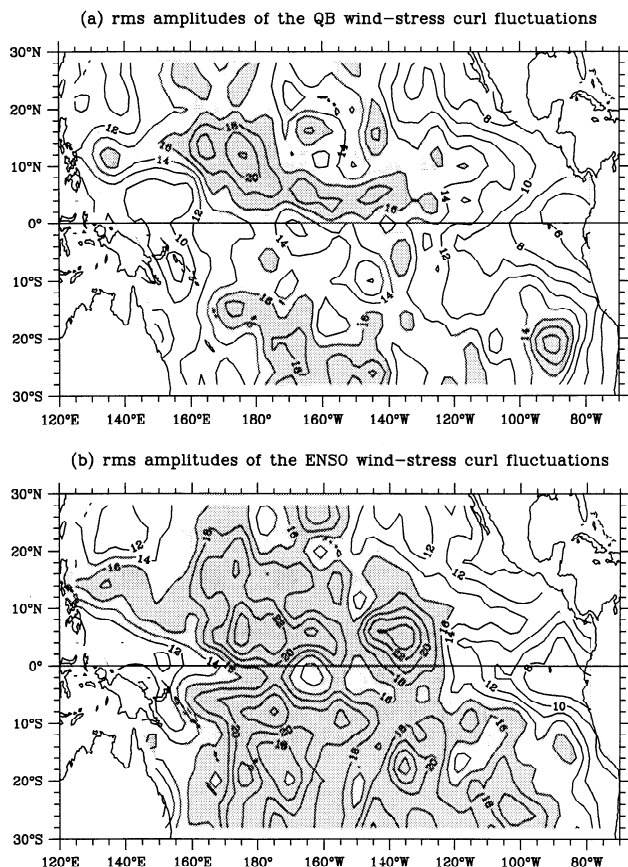


Figure 15. Root-mean-square amplitudes of the wind stress curl fluctuations in (a) the quasi-biennial ($1.8 < \text{period} < 2.2$ years) and (b) the El Niño-Southern Oscillation ($3 < \text{period} < 7$ years) frequency bands. Values are calculated from the monthly FSU wind data from 1961 to 1992. Areas with rms amplitude values greater than $16 \times 10^{-9} \text{ N m}^{-3}$ are stippled.

For the current transports we found that the seasonal fluctuations of the NEC near the western boundary (± 3.3 Sv, see Table 1) are relatively small as compared with the seasonal fluctuations of the Kuroshio (± 5.5 Sv) and the Mindanao Current (± 4.9 Sv). This is because the seasonal wind-driven fluctuations in the Kuroshio and the Mindanao Currents are nearly 180° out of phase due to the different phase speed of the baroclinic Rossby waves at their respective latitudes. The Kuroshio (the Mindanao Current) attains its maximum transport in spring (fall) and its minimum transport in fall (spring). This model result on the seasonal changes of the NMK system is in agreement with the observational result presented by *Wyrtki* [1961]. Notice that the minimum (maximum) Kuroshio transport in fall (spring) coincides with the northernmost (southernmost) bifurcation of the NEC along the Philippine coast.

In the interannual frequency band many of the transport increases of the NEC near the western boundary can be linked to the ENSO. During the mature phase of an El Niño the NEC tends to intensify due to the strengthening of the northeast trade wind (see also *Mitchum* [1987]). There exist, however, years in which the transport increase is caused by the wind anomalies that are confined to the western low-latitude Pacific but are not related to the warming in the eastern equatorial Pacific. A salient example of this is in 1980, in which an intense NEC is observed both in the model simulation and in the in-situ data. The transport fluctuations of the Mindanao Current are found to be coherent with those of the NEC on timescales of 2–7 years. In contrast, the coherence between the transports of the NEC and the Kuroshio is low on the quasi-biennial timescale. Analyzing the FSU wind data in the frequency domain revealed that the quasi-biennial changes in the surface wind stress curl field are mainly confined to the low-latitude, western Pacific, a forcing pattern explaining the confinement of the quasi-biennial oscillations in the southern limb of the NMK current system. On ENSO timescales (3–7 years), however, the transport fluctuations of the NEC are found to pass coherently into the northward flowing Kuroshio. This suggests that some of the low-latitude ENSO signals penetrate into the mid-latitude circulation through the western boundary current of the subtropical gyre.

In this model there is no throughflow from the Pacific Ocean to the Indian Ocean. The potential influence of the closure of the throughflow on our results must be considered because it relates to the role of the western boundary considered in this study. Here we can appeal to the work by *Verschell et al.* [1995], who made calculations with a model (similar to the one used here) in which results from both open and closed Indonesian Seas were compared. Shutting off the 7.5 ± 4.8 Sv of throughflow results in major changes to the Indian Ocean and smaller changes in the Pacific. The region of the Mindanao Eddy (5° – 10° N, 130° E) is affected. The differences between open and closed throughflow cases

show both high- and low-frequency variability, though much of the rms difference has periods shorter than 1/2 year. Thus the absence of the Indonesian throughflow in the present model may influence the Mindanao Current transport fluctuations somewhat, but the differences are confined to the region south of 10° N and are largely concerned with the mesoscale eddy generation in this region. Thus our conclusion regarding the NEC bifurcation and the transport fluctuations of the Kuroshio and NEC are robust with respect to the absence of the throughflow. Our conclusions regarding the transport fluctuations of the Mindanao Current are unlikely to be modified in a qualitative sense, though quantitative differences are likely.

Finally, we note that the seasonal and interannual changes of the NMK system obtained in this study result strictly from dynamical responses to the surface wind forcings. This does not imply that thermodynamically induced changes in the NMK system are small or unimportant. To better understand the NMK system and its roles in the regional climate and in the large-scale tropical-subtropical circulations, future studies including surface buoyancy forcings are required.

Acknowledgments. This study benefited from many discussions with Peter Hacker, Fei-fei Jin, William Kessler, Julian McCreary, Michael McPhaden, and James Potemra. Careful reviews by John Toole and an anonymous reviewer improved many parts of an early version of the manuscript. The sea level data used in this study are provided by the TOGA Sea Level Center at the University of Hawaii and the surface wind data by Florida State University. B.Q. was supported by the National Science Foundation through grant OCE94-03048. R.L. was supported by the NSF through grant OCE92-24452.

References

- Arakawa, A., and V.R. Lamb, Computational design of the basic dynamical processes of the UCLA General Circulation model, *Methods Comput. Phys.*, **17**, 173–265, 1977.
- Barnett, T.P., The interaction of multiple time scales in the tropical climate system, *J. Clim.*, **4**, 269–285, 1991.
- Bingham, F.M., and R. Lukas, The southward intrusion of North Pacific Intermediate Water along the Mindanao coast, *J. Phys. Oceanogr.*, **24**, 141–154, 1994.
- Busalacchi, A.J., and J.J. O'Brien, The seasonal variability in a model of the tropical Pacific, *J. Phys. Oceanogr.*, **10**, 1929–1951, 1980.
- Busalacchi, A.J. and J.J. O'Brien, Interannual variability in a model of the tropical Pacific in the 1960s, *J. Geophys. Res.*, **86**, 10,901–10,907, 1981.
- Cannon, G.A., Characteristics of waters east of Mindanao, Philippine Islands, August 1965, Contrib. 120, pp.205–211, Chesapeake Bay Inst. and Dep. of Oceanogr., Johns Hopkins Univ., Baltimore, Md., 1970.
- Church, J.A., The East Australian Current adjacent to the Great Barrier Reef, *Aust. J. Mar. Freshwater Res.*, **38**, 671–683, 1987.
- Donguy, J.R., C. Henin, A. Morliere, and G. Meyers, Appearances in the western Pacific of phenomena induced by El Niño in 1979–80, *Trop. Ocean Atmos. Newsl.*, **10**, 1–2, 1982.
- Goldenberg, S.R., and J.J. O'Brien, Time and space variability of tropical Pacific wind stress, *Mon. Weather Rev.*, **109**, 1190–1207, 1981.

- Fine, R.A., R. Lukas, F.M. Bingham, M.J. Warner, and R.H. Gammon, The western equatorial Pacific: A water mass crossroads, *J. Geophys. Res.*, *99*, 25,063–25,080, 1994.
- Hellerman, S., and M. Rosenstein, Normal monthly wind stress over the world ocean with error estimates, *J. Phys. Oceanogr.*, *13*, 1093–1104, 1983.
- Hu, D., and M. Cui, The western boundary current of the Pacific and its role in the climate, *Chin. J. Oceanol. Limnol.*, *9*, 1–14, 1991.
- Inoue, M., and S.E. Welsh, Modeling seasonal variability in the wind-driven upper-layer circulation in the Indo-Pacific region, *J. Phys. Oceanogr.*, *23*, 1411–1436, 1993.
- Kessler, W.S., Observations of long Rossby waves in the northern tropical Pacific, *J. Geophys. Res.*, *95*, 5183–5217, 1990.
- Kindle, J., H. Hurlburt, and J. Metzger, On the seasonal and interannual variability of the Pacific to Indian Ocean throughflow, paper presented at *Western Pacific International Meeting and Workshop on TOGA COARE*, Inst. Fr. de Rech. Sci. pour le Dev. en Coop. (ORSTOM), Noumea, New Caledonia, 1989.
- Kubota, M., and J.J. O'Brien, Variability of the upper tropical Pacific Ocean model, *J. Geophys. Res.*, *93*, 13,930–13,940, 1988.
- Lighthill, M.J., Dynamic response of the Indian Ocean to onset of the southwest monsoon, *Philos. Trans. R. Soc. London A*, *265*, 45–92, 1969.
- Lukas, R., Interannual fluctuations of the Mindanao Current inferred from sea level, *J. Geophys. Res.*, *93*, 6744–6748, 1988.
- Lukas, R., E. Firing, P. Hacker, P.L. Richardson, C. A. Collins, R. Fine, and R. Gammon, Observations of the Mindanao Current during the Western Equatorial Pacific Ocean Circulation Study, *J. Geophys. Res.*, *96*, 7089–7104, 1991.
- Masumoto, Y., and T. Yamagata, Response of the western tropical Pacific to the Asian winter Monsoon: The generation of the Mindanao Dome, *J. Phys. Oceanogr.*, *21*, 1386–1398, 1991.
- McCreary, J.P., and P. Lu, On the interaction between the subtropical and the equatorial oceans: The Subtropical Cell, *J. Phys. Oceanogr.*, *24*, 466–497, 1994.
- McPhaden, M.J., A.J. Busalacchi, and J. Picaut, Observations and wind-forced model simulations of the mean seasonal cycle in tropical Pacific sea surface topography, *J. Geophys. Res.*, *93*, 8131–8146, 1988.
- Meehl, G.A., The annual cycle and interannual variability in the tropical Pacific and Indian Ocean regions, *Mon. Weather Rev.*, *115*, 17–50, 1987.
- Meyers, G., On the annual Rossby wave in the tropical North Pacific, *J. Phys. Oceanogr.*, *9*, 663–674, 1979.
- Metcalf, W.G., Shallow currents along the northeastern coast of South America, *J. Mar. Res.*, *26*, 232–243, 1968.
- Mitchum, G.T., Trade wind fluctuations associated with El Niño–Southern Oscillation, *J. Geophys. Res.*, *92*, 9464–9468, 1987.
- Nitani, H., Beginning of the Kuroshio, in *Kuroshio: Its Physical Aspects*, edited by H. Stommel and K. Yoshida, 129–163, Univ. of Tokyo Press, Tokyo, 1972.
- Philander, S.G.H., W.J. Hurlin, and A.D. Seigel, Simulation of the seasonal cycle of the tropical Pacific Ocean, *J. Phys. Oceanogr.*, *17*, 1986–2002, 1987.
- Qiu, B., and T. Joyce, Interannual variability in the mid- and low-latitude western North Pacific, *J. Phys. Oceanogr.*, *22*, 1062–1079, 1992.
- Sadourny, R., The dynamics of finite-difference models of the shallow-water equations, *J. Atmos. Sci.*, *32*, 680–689, 1975.
- Toole, J.M., E. Zou, and R.C. Millard, On the circulation of the upper waters in the western equatorial Pacific Ocean, *Deep Sea Res., Part A*, *35*, 1451–1482, 1988.
- Toole, J.M., R.C. Millard, Z. Wang, and S. Pu, Observations of the Pacific North Equatorial Current bifurcation at the Philippine coast, *J. Phys. Oceanogr.*, *20*, 307–318, 1990.
- Verschell, M.A., J.C. Kindle, and J.J. O'Brien, Effects of Indo-Pacific throughflow on the upper tropical Pacific and Indian Oceans, *J. Geophys. Res.*, *100*, 18,409–18,420, 1995.
- Wijffels, S.E., E. Firing, and J. Toole, The mean structure and variability of the Mindanao Current at 8°N, *J. Geophys. Res.*, *100*, 18,421–18,435, 1995.
- Wyrtki, K., Physical oceanography of the southeast Asian waters, NAGA Rep.2, 195 pp., Scripps Inst. of Oceanogr., Univ. of Calif. San Diego, La Jolla, 1961.
- Yamagata, T., Y. Shibao, and S. Umatani, Interannual variability of the Kuroshio Extension and its relation to the Southern Oscillation/El Niño, *J. Oceanogr. Soc. Jpn.*, *41*, 274–281, 1985.
- Yasunari, T., A possible link of the QBOs between the stratosphere, troposphere and sea surface temperature in the tropics, *J. Meteorol. Soc. Jpn.*, *67*, 483–493, 1989.

R. Lukas and B. Qiu, Department of Oceanography, University of Hawaii at Manoa, 1000 Pope Rd., Honolulu, HI, 96822. (e-mail: rlukas@iniki.soest.hawaii.edu, bqiu@iniki.soest.hawaii.edu)

(Received February 2, 1995; revised September 26, 1995; accepted September 28, 1995.)